Effect of salinity on the microscopic interaction and sedimentation behavior of halloysite clay

Namgyu Noh
Korea Advanced Institute of Science and Technology https://orcid.org/0000-0002-0427-3757
Yeong-Man Kwon
Korea Advanced Institute of Science and Technology
Kyun Seong Dae
LG Energy Solution https://orcid.org/0000-0001-5928-9855
Gye-Chun Cho
Korea Advanced Institute of Science and Technology
Ilhan Chang
Ajou University
Jong Min Yuk (jongmin.yuk@kaist.ac.kr)
Korea Advanced Institute of Science and Technology

Article

Keywords: HNT, salinity, sedimentation, flocculation, in-situ liquid-phase microscopy

Posted Date: March 14th, 2022

DOI: https://doi.org/10.21203/rs.3.rs-1421994/v1

Abstract

Pore-fluid salinity has a predominant effect on the formation of soil suspensions, especially for clays adjacent to the ocean, including bays, lagoons, sounds, slough, and estuaries. However, the clay response to changes in pore fluid salinity (e.g., salt intrusion or extrusion) has yet to be investigated. Herein, the influence of salinity on the microscopic interaction and sedimentation behavior of halloysite clay was investigated in an aqueous condition. Macro-scale sedimentation experiments and *in-situ* microscopic observations showed that halloysite clays in pore fluids with high ionic strength tended to disperse because salt ions weaken the edge-to-face halloysite fabrics. In the ensuing drop of the salinity, salt ions adsorbed onto the double layer of the clay surface were not reversely released. Comparing to sediment with a similar initial salinity, desalination resulted in weakened edge-to-face structures (a lower initial settling rate) and loose final sediment (a higher final sediment void ratio). Our study provides a thorough understanding of the salt effect on sediment formation, including changes in the microscopic clay particle fabric as salinity changes.

Introduction

Dispersed clay particles in the solution state flocculate and settle down by gravitational and electrical forces [1]. The soil settling behavior is important for identifying sediment accumulation [2], reclamation [3], disposal of mineral wastes [4], river-floodplain morphodynamics [5], colloidal chemistry [6], and wastewater treatment [7]. Various empirical and theoretical approaches have identified clay particle interaction mechanisms and settling behaviors [1, 8, 9, 10, 11]. Complex parameters such as particle size, sediment concentration, and organic and chemical environments influence the settling behavior of clay particles in aqueous suspension [12, 13]. In general, greater particle size, container size, specific weight of sediment, and net particle attraction force cause sediments to settle faster, while higher particle hindrance and fluid viscosity conditions cause sediments to settle slower [10, 14, 15].

Because clay minerals have surface charge characteristics, the interaction and sedimentation behavior of clays is governed by net interparticle forces (i.e., double-layer force, van der Waals force, and other forces described by DLVO theory) [16, 17, 18]. The chemical properties of the pore fluid (e.g., pH and salinity) have an impact on clay surface charges and net forces between clay particles [8, 19, 20]. Clay minerals are composed of a pH-independent or -dependent charge based on the protonation-deprotonation of broken bonds in the alumina layer [21, 22]. Because the edge surface is positively charged, clay particles prefer to form edge-to-face (EF) fabrics when the pH is below the isoelectric point of the edge surface [23, 24]. In contrast, the double-layer repulsion between all-negative clay surfaces regulates the clay interaction at a pH greater than the isoelectric point of the edge surfaces. Based on these findings, Wang and Siu [9] observed a decrease in the settling velocity and an increase in the final sediment density with an increase in the pH of kaolinite suspensions.

Salt-induced double-layer compression affects the net interparticle forces. For example, as pore-fluid salinity increases, the repulsion force between two surfaces with identical charges (face-to-face; FF) tends to decrease [25]. In addition, salinity reduces the attraction force (double layer force, Coulomb attraction) between oppositely charged surfaces (EF) [9, 24, 26]. On the other hand, van der Waals forces vary in a non-linear manner with the fluctuation in the dielectric constant of the pore media [27, 28, 29]. In other words, depending on the pore fluid chemistry, the pore-fluid salinity strengthens or weakens particle attachments. Therefore, the surface charge heterogeneity of clay minerals makes it difficult to interpret the interactions between clay particles.

Here, we analyzed the sedimentation behaviors of halloysite clay nanotubes (HNTs) and visualized the self-assembly behaviors of clay particles at flocculation states using liquid-phase microscopy techniques. Colloidal stability (i.e., dispersed fabrics, lower settling velocity) is critical when using HNTs for drug delivery and gas storage and release purposes [30], while coagulation and flocculation (i.e., flocculated fabrics, higher settling velocity) are significant factors for wastewater treatment [31]. Sediment transport and sedimentation in rivers and reservoirs are also dependent on settling velocity, which changes depending on particle formation [32]. Thus, understanding the fabric interaction with different pore fluid chemistry is crucial for HNTs' industrial applicability. We also discovered the hidden irreversible flocculation and sedimentation behaviors corresponding to the permanent double layer compression under salinity exchange conditions. Based on the outcomes of this investigation, we established a relationship between clay mineral flocculation and sedimentation.

Results

Sedimentation behavior of halloysite clay nanotubes (HNTs) at different initial salinity

This study observed the salinity effect on the settling of the HNTs. The HNTs are omnipresent clay minerals formed from volcanic, tropical, and pre-glacially weathered materials [33]. Unlike the plate morphology of ordinary clay minerals (e.g., kaolinite, smectite), HNTs have a tubular shape (Supplementary Fig. 1), which is created by a mismatch between alumina and silica sheets, the attraction between interlayer hydroxyl groups in alumina octahedrons, and the surface tension of water [34]. As a result, the HNTs have different inner/outer space chemistries, with the outer space composed of silica tetrahedron (SiO_4), negatively charged regardless of pH, and the inner and edge areas composed of alumina octahedron ($Al(OH)_6$) group, positively charged in a pH range of 2–8 [30, 35, 36,37]. The pH level of the supernatant water was maintained in the range of 3.5-5.0 [36] to preserve the surface chemistry, and the edge surface of HNTs had a positive charge [37] (Supplementary Fig. 2). The temporal salinity variation was simulated by replacing the supernatant liquids after a single sedimentation process where pore-fluid salinity increased (i.e., salination stage) from 0 M to 0.6 M NaCl and gradually decreased to 0.01 M NaCl (i.e., desalination stage).

Figure 1 shows a representative sedimentation behavior of HNTs in suspension under a sequential liquid exchange environment. In the solution, the well-dispersed HNT particles naturally interact through electrostatic forces during the settling. The HNT particles experience self-assembly and spontaneously form the deposits. We observed that the HNTs gravitate to the bottom and agglomerate together at the overall salinity condition within hours (Fig. 1a and Supplementary Fig. 2). Higher salinity resulted in lower initial settling velocity and higher sediment density during the salination stage (Fig. 1b and c). These sedimentation features are well explained by net interaction forces in a colloidal system with NaCl additive.

The interaction among colloidal particles has been described by the DLVO model, which describes the combination of van der Waals attraction and electrostatic Coulomb forces [17]. We calculated the total interaction energy as a function of separation distance and interaction sites between the HNT particles with anisotropic charge distribution according to $V = V^{HHF} + V^{LW}$, where V is total interaction energy, V^{HHF} is the double layer energy [38], and V^{LW} is van der Waals energy [39], respectively. Based on the calculation in pure liquid (Supplementary Fig. 3), the net charge potential of HNTs with identical negative charge surface (FF interaction) has a substantial energy barrier near 10 nm of separation distance by repulsion force. On the other hand, the EF and EE (edge-to-edge) structures have attractive interaction (electrostatic or van der Waal attraction) dominant net potential features in the calculation scale. In the salinity increase cases (Supplementary Fig. 4), all particle interaction is suppressed by double-layer compression of dispersed salt ions near the clay surface [40]. Notably, salt addition effectively reduced the attraction between oppositely charged clay surfaces (EF attraction) (Supplementary Fig. 5). These results show that HNTs with higher salinity form a more dispersed state in their initial settling state and are stacked by FF fabrics. In general, sediments settle faster as particle and floc sizes increase [10, 14, 15]. It means that when the salinity increases, small or dispersed particles form, lowering the initial settling velocity while increasing the final sediment density.

In contrast, the settling behavior during desalination did not appear to be repeatable under the same salinity conditions at the preceding salination stage. Specifically, the initial settling velocity (Fig. 1b) slightly increased during desalination (Steps 6–9) but did not return to the initial settling velocity level during the early salination stage for each corresponding salinity case (Fig. 1b). Meanwhile, the desalination process increased the final sediment void ratio (Fig. 1c) compared to its counterpart salinity condition under salination. Remarkably, in the reverse case of salinity variation where salinity dropped (desalination from 0.6 M NaCl to 0.01 M NaCl) and then elevated again (salination up to 0.6 M NaCl), the settling behavior of HNTs showed symmetrical variation (Supplementary Fig. 6). The sedimentation only becomes irreversible when the salt level varies from salination to desalination process. It meant that the salt-induced permanent double-layer reduction happened during the prior salination process. Previous studies have also reported an irreversible sedimentation behavior with salinity [41] and pointed out that the sedimentation process with flocculation resulted in a higher void ratio of natural clay deposits [2]. The salt additives actively influence the aggregation behavior of HNTs even under salt removing conditions. It can

be assumed that the residual salt affects the clay fabrics, resulting in fabrics with open and larger voids. Therefore, visual observation of fabric flocculation during settling is required.

Fundamental flocculation behavior among HNTs

To visualize the sedimentation behavior in HNT suspension, we facilitated the *in-situ* liquid-phase scanning electron microscopy (LPSEM). The SiN_x based liquid flowing system can provide the initial settling stage due to dispersed particle injection by the confined liquid reservoir and liquid injection channel. We performed image processing on the acquired image to obtain a clear floc region, following filtering and binarization (Supplementary Fig. 7). Figure 2a shows the floc formation of the HNTs in suspensions at different initial salinity conditions. In the liquid chamber, electrostatic forces assemble the HNTs. The HNT particles (Gray region) and water molecules (Black region) that make up the floc structures are generated as a function of salinity. At low salinity, the HNT building blocks assemble to form a large aggregate. Although the floc shapes are atypical, the microstructure of aggregates consist of HNT networks with unit EE and EF associations. On the other hand, the projected floc areas are decreased from ~ 2.0 μm^2 to ~ 0.5 μm^2 as increasing salinity from 0.01 M to 0.6 M (Fig. 2b). At 0.6 M salt concentration, the average particle size reaches a few particle levels corresponding to HNT size (Supplementary Fig. 1). Smaller flocs result from an increase in salinity, and the HNT networks in the floc are significantly reduced. The tendency toward dispersion as salinity rises implies that electrostatic interaction between HNT particles decreases due to a reduction in double layer thickness as salt concentration increases.

To reveal the fundamental interaction between particles in floc, we performed *in-situ* liquid-phase transmission electron microscopy (LPTEM) observation to visualize the microscopic self-assembly processes among HNT particles in suspension. This method can imitate the particle to particle association due to the confined SiN_x liquid flow system. The HNT particles could be distinguished in an aqueous (DI water) environment, demonstrating the fundamental formation pathways of floc fabrics at an earlier stage. Hence, we tracked the newly formed fabrics over the entire infusion experiment. Figure 3a shows the real-time LPTEM images of the flocculation events between HNT particles in the suspension (Video 1). When we started observation in the target window, we observed the projected structure of the preformed fabric composed of HNT particles with dark contrast before electron beam exposure (at t = 0 s). The particles are dispersed throughout the flowing channel, where they may interact with adjacent particles or aggregates. When particles interact with each other through thermally random motion or flowing forces, particles prefer to form a floc structure to reduce the net interaction energy (Supplementary Fig. 3). The majority of microstructures exhibit a complex architecture mainly composed of the EE and EF associations (Supplementary Fig. 8), which have been proposed as common mechanisms for creating clay networks [4]. However, FF assembly is rarely observed due to the repulsive field between double layers with identical charge [42] (Supplementary Fig. 3). The floc structures initiated by attachments of HNTs and EE/EF-based association increase continuously as increasing injection time (Supplementary Fig. 9).

According to the experiment, detailed flocculation pathways can be categorized into two main associations: EE and EF unit structure. We show the typical examples of HNT assemblies as formation process in Fig. 3b-g (other flocculation cases present in Supplementary Fig. 10). Basically, a pairing of HNTs is initiated by attachment of the directly injected particle, as depicted in case 1 in Fig. 3b, c, and d (Video 2, 3 and 4). The supplied particle is directly contacted at the edge or face of the preformed objects. By van der Waals and electrostatic attraction, the HNT assembly mainly picks the EE or EF structure (Supplementary Fig. 3). Meanwhile, the separated particle, which has moved away from the original bound states, can transfer to a new contact state with nearby particles (Supplementary Fig. 10 and video 8, 9).

However, the typical structures of HNT assemblies involve complex networks through interlocked multiple contacts and pairwise contact. A nanotube fixed on the edge site of HNT can move in an angular direction by liquid flowing (Case 2 in Fig. 3e, f and video 5, 6). The moving rod is contacted at the edge or face of another particle when the rod approaches another particle. A double contacted structure can form to minimize the net interaction energy. This can be permitted for the floc to floc assembly process (Case 3 in Fig. 3g and video 7). The aggregates, developed outside the viewing area by the long infusion length, directly attach the preformed assembly with multiple EE and EF connections. Consequently, the floc size grew as a result of the attachment processes. The particle interaction is efficiently regulated to minimize the net interaction energy in the liquid system, according to these dynamical processes of HNTs. By consecutive particle and floc attachment in the settling stage, multidimensional HNT frameworks are created.

HNT interactions at the salinity exchange conditions

We discovered macro-scale aggregated HNTs via a series of salination (0.01 M → 0.1 M → 0.3 M → 0.6 M) and desalination (0.6 M → 0.3 M → 0.1 M → 0.01 M) exchange procedures using liquid-phase optical microscopy (LPOM) during the salination and desalination process (method and Fig. 4a). After particles settle down in droplets, the average floc size decreases from 7 μm to 6.1 μm as increasing salinity. This situation is induced by the reduction of a double layer. However, with decreasing salinity, the floc sizes increase from 6.1 μm to 7.7 μm (Fig. 4b).

Remarkably, the LPOM observation of HNT aggregates as salinity decreases demonstrates an irreversible size variation trend matching sedimentation behavior. During the desalination process, suspended particles may assemble each other as an increasing double layer on the periphery of the HNT. However, a decrease of salt concentration leads to low density and low settling velocity despite the large floc size about HNT assembly (Figs. 1 and 4c). To understand unpredicted behavior, we consider the role of salt in the colloid. Na^+ ion has a low affinity with silica tetrahedron of HNT surface in low ionic strength, and it only forms a broad diffusion layer on the periphery of HNTs. However, we used 0.6 M in salinity in our system, and Na^+ ion can create a dense ionic cloud onto a negatively charged surface [43]. The Na^+ ion prefers to be directly linked to the silica tetrahedron outer sphere or defective sites of HNT with high ionic strength [44], causing permanent screening of surface charge of HNT.

Because of the directly coupled structure with the outer HNT surface, the salt ions adhering to the surface are not completely removed when the salt concentration is lowered. Consequently, when salinity returns to a salt concentration with low ionic strength, electrostatic (EF interaction) attraction with opposite charge may be weakened compared to the initial experimental condition, whereas the EE attraction with van der Waals is unaffected. The EE interaction formed a honeycomb structure with the largest pore volume in aggregate structure compared to EF-induced structure (Fig. 4c). It produces open sediment with a strewn-together stacking structure. These results indicate that the residual salt ion on the HNT surface is effectively worked to the particle to particle interaction by pore salinity variation. In other words, salinity changes throughout the settling process in the colloidal system might permanently alter the initial flocculation and sedimentation structure of HNT minerals.

Discussion

Multiscale analysis was used to explore the sedimentation behavior and interparticle interaction of HNTs in this study, which included *in-situ* liquid microscopic observations and sedimentation tests of soil mass. We propose the following correlation between HNTs from flocculation to sedimentation as salinity variation based on macro sedimentation tests and *in-situ* observations: At low salinity, the HNTs assemble by Coulombic (EF association with opposite charge) and van der Waals (EE association) attraction to minimize net interaction energies. It forms large aggregates with card house structures, composed of EF-dominant densely packed structures. Thus, the aggregates result in higher settling velocity and low-density sediment.

The double layer field of HNTs is compressed by concentrated salt ions as salinity increases, and particle interaction is effectively suppressed. Hence, decreased particle contact can reduce the particle size and cause particle dispersion during settling. This results in a low settling rate and higher sediment density with physically close-packed FF stacks. In contrast, when salt concentration with low ionic strength is recovered, the Na^+ ions are not completely removed from the HNT surface and may induce persistent compression of the double layer field of the face side. As a result, the micro floc structures are transformed into loosely packed EE-dominant honeycomb structures. This can lead to forming a larger and more open floc. As a result of the variations in microstructure induced by the remaining salt, the settling speed becomes slower and the sediments are more open and low density than in the original conditions.

Our findings revealed the crucial role of clay minerals and salt additives in the correlation of flocculation and sedimentation behaviors in a liquid environment. The salt additives provide a suppression nature of clay mineral interaction. When the salinity is adjusted, it creates a change of the permanent charge configuration at the clay mineral surfaces. This is one of the most important aspects of comprehending the fundamental mechanisms that govern the micro-and macro-structure of clay minerals in nature as salinity varies. The interaction features of clay nanoparticles may bring new insight into controlling the electrochemical or physical properties of clay minerals for the specific application.

Methods

Sample information

This study used halloysite, an aluminosilicate clay mineral, with the empirical formula $Al_2Si_2O_5(OH)_4 \cdot nH_2O$. Supplementary Figure 1a shows the particle size distribution of halloysite observed using a laser scattering particle size analyzer (HELOS/KR, Sympatec GmbH, Germany). Over 50% of the halloysite had a sediment size smaller than 6.16 μm. The tubular morphologies of dried HNT particles were confirmed using SEM (SU5000, Hitachi) and TEM (JEM-3010, JEOL) (Supplementary Fig. 1b and 1c). Element mapping analysis was performed to confirm the composition of dried HNT by using JEM-ARM200CF (JEOL) equipped with energy dispersive X-ray (EDX) detectors. The Al, Si, and O were uniformly distributed in tubular HNT particles (Supplementary Fig 1d). A research-graded HNT (Merck, CAS: 1332-58-7) without further purification was used.

Preparation of clay suspensions

The HNT fabrics of suspension with high water content (m_w/m_s, [1,000 %]) were assessed from the settlement behavior, measured with time from the initial suspension stage until the HNT sediment reached a constant volume. A graduated cylinder (60 mm in diameter and maximum volume of 1,000 mL) was filled with 100 ml of the test fluid. Sodium chloride (NaCl) was used to prepare fluids with different salinity conditions (from 0 to 0.6 M) by dissolving 99.5% pure NaCl (CAS: 7647-14-5; Junsei Chemical Co., LTD., Japan) in deionized water. HNTs (90 g; 35 mL in volume) were poured into the cylinder with 100 mL of test fluid and mixed to form a condensed suspension. Then, additional test fluid was poured into the cylinder to reach a final volume of 935 mL. The HNT suspension was slowly mixed by shaking upside down until a uniform suspension was obtained. The prepared suspensions were rested for 24 h for full hydration. A thermoplastic film (Parafilm M, USA) capped the top of the cylinders for sealing and wrapping. Then, fully hydrated HNT suspensions were vigorously disturbed for at least 1 min by shaking and inverting each sealed cylinder upside down. The cylinders were placed on a level surface after the last inversion, and this was regarded the commencement of sedimentation (time = 0). The sediment height was tracked over time until the final sediment height reached a constant volume with a settlement rate of less than 1.0 mL/day. A single sedimentation period could last up to seven days.

After the sediment reached a constant height, the supernatant water was removed, and the cylinder was refilled to 935 mL with a fluid having a different salinity, using a pipette (WI.5.381.000; Witeg, Germany) to represent salination or desalination conditions. After each procedure, the pH and electrical conductivity of the supernatant were measured using a pH/conductivity meter (S470-USP-K; Mettler Toledo, USA).

In-situ liquid microscopy

HNT powders were fractionated to investigate the microscopic interactions using *in-situ* electron microscopy, with the gravitational methods developed by M. L. Jackson [45], which help filter agglomerated particles >2 μm. Then, to obtain the monodispersed suspension, filtered HNTs were dispersed in water (10 mM) using a tip-sonicator, VCS-750 (Sonics & Materials, Inc.). To differentiate the individual particles in confinement, we used a low concentration in suspension, which provides the flocculation behavior of the initial stage.

To investigate the microscopic insights into the associations of HNTs, we introduced *in-situ* liquid cell microscopy systems, which enabled us to record the time-series events of the flocculation formation and particle association change in response to a change in the solution environment and salinity. JEM-3010 (JEOL) equipped with the USC1000 (Gatan) camera and a Poseidon holder (Protochips) was used to observe the real-time LPTEM measurements at an acceleration voltage of 300-kV. The liquid chamber equipped in Poseidon holder consisted of SiN_x membrane-based liquid cell with ~ 50 nm height and 2 × 2 mm^2 space. HNTs were infused into the liquid holder system to resolve the flocculation process from a particulate point of view using the Pump 11 Elite Syringe Pumps (Harvard Apparatus), with an infusion rate of 0.5 μL/min. Sigma 300 (Carl ZEISS).

A homemade liquid-cell SEM holder was used to visualize the flocculation behavior at different salinity levels. The chamber dimension of LPSEM is ~1 μm in height and 2 × 2 mm^2 space. We gathered a series of snapshots, which corresponded to the different salinity: 0.01 M, 0.1 M, 0.3 M, and 0.6 M.

For monitoring of HNT aggregates under the salinity exchange condition, we used optical microscopy (LPOM; Olympus). It was observed after suspension dropped onto the slide glass at each salinity after salinity exchange from salination (from 0.01 M to 0.6 M) to desalination (from 0.6 M to 0.01 M).

Data availability

All necessary data generated or analyzed during this study are included in this published article, and other auxiliary data are available from the corresponding authors upon request.

References

1. Kynch GJ. A theory of sedimentation. Transactions of the Faraday Society **48**, 166–176 (1952).
2. Watabe Y, Saitoh K. Importance of sedimentation process for formation of microfabric in clay deposit. Soils and Foundations **55**, 276–283 (2015).
3. Lee SL, Karunaratne GP, Yong KY, Ganeshan V. Layered clay-sand scheme of land reclamation. Journal of Geotechnical Engineering **113**, 984–995 (1987).
4. Zbik MS, Smart RSC, Morris GE. Kaolinite flocculation structure. J Colloid Interf Sci **328**, 73–80 (2008).

5. Lamb MP, *et al.* Mud in rivers transported as flocculated and suspended bed material. Nature Geoscience **13**, 566–570 (2020).
6. Lagaly G, Ziesmer S. Colloid chemistry of clay minerals: the coagulation of montmorillonite dispersions. Adv Colloid Interfac **100–102**, 105–128 (2003).
7. Shaikh SMR, Nasser MS, Hussein I, Benamor A, Onaizi SA, Qiblawey H. Influence of polyelectrolytes and other polymer complexes on the flocculation and rheological behaviors of clay minerals: A comprehensive review. Separation and Purification Technology **187**, 137–161 (2017).
8. Sridharan A, Prakash K. Influence of clay mineralogy and pore-medium chemistry on clay sediment formation. Can Geotech J **36**, 961–966 (1999).
9. Wang YH, Siu WK. Structure characteristics and mechanical properties of kaolinite soils. I. Surface charges and structural characterizations. Can Geotech J **43**, 587–600 (2006).
10. Imai G. Settling behavior of clay suspension. Soils and Foundations **20**, 61–77 (1980).
11. Kwon Y-M, Im J, Chang I, Cho G-C. ε-polylysine biopolymer for coagulation of clay suspensions. Geomech Eng **12**, 753–770 (2017).
12. Berlamont J, Ockenden M, Toorman E, Winterwerp J. The characterisation of cohesive sediment properties. Coastal Engineering **21**, 105–128 (1993).
13. Chang I, Cho GC. A New Alternative for Estimation of Geotechnical Engineering Parameters in Reclaimed Clays by Using Shear Wave Velocity. Geotech Test J **33**, 171–182 (2010).
14. Chamley H. *Clay sedimentology*. Springer, Berlin, Heidelberg (2013).
15. Toorman EA. Sedimentation and self-weight consolidation: general unifying theory. Géotechnique **46**, 103–113 (1996).
16. Verwey EJW. Theory of the Stability of Lyophobic Colloids. The Journal of Physical and Colloid Chemistry **51**, 631–636 (1947).
17. Missana T, Adell A. On the applicability of DLVO theory to the prediction of clay colloids stability. J Colloid Interf Sci **230**, 150–156 (2000).
18. van Oss CJ, Giese RF, Costanzo PM. DLVO and Non-DLVO Interactions in Hectorite. Clay Clay Miner **38**, 151–159 (1990).
19. Kotylar LS, Sparks BD, Schutte R. Effect of Salt on the Flocculation Behavior of Nano Particles in Oil Sands Fine Tailings. Clay Clay Miner **44**, 121–131 (1996).
20. Durán JDG, Ramos-Tejada MM, Arroyo FJ, González-Caballero F. Rheological and Electrokinetic Properties of Sodium Montmorillonite Suspensions: I. Rheological Properties and Interparticle Energy of Interaction. J Colloid Interf Sci **229**, 107–117 (2000).
21. Mohan KK, Fogler HS. Effect of pH and layer charge on formation damage in porous media containing swelling clays. Langmuir **13**, 2863–2872 (1997).
22. Tombácz E, Szekeres M. Surface charge heterogeneity of kaolinite in aqueous suspension in comparison with montmorillonite. Appl Clay Sci **34**, 105–124 (2006).
23. Rand B, Melton IE. Isoelectric point of the edge surface of kaolinite. Nature **257**, 214–216 (1975).

24. Rand B, Melton IE. Particle interactions in aqueous kaolinite suspensions: I. Effect of pH and electrolyte upon the mode of particle interaction in homoionic sodium kaolinite suspensions. J Colloid Interf Sci **60**, 308–320 (1977).
25. Israelachvili JN. *Intermolecular and surface forces*, 3rd edn. Academic press (2011).
26. Miklavic SJ, Chan DY, White LR, Healy TW. Double-Layer Forces Between Heterogeneous Charged Surfaces. Journal of Physical Chemistry **98**, 9022–9032 (1994).
27. Chen J, Anandarajah A. Influence of Pore Fluid Composition on Volume of Sediments in Kaolinite Suspensions. Clay Clay Miner **46**, 145–152 (1998).
28. Anandarajah A, Chen J. Van Der Waals Attractive Force Between Clay Particles in Water and Contaminants. Soils and Foundations **37**, 27–37 (1997).
29. Somasundaran P, Mehta SC, Yu X, Krishnakumar S. *Colloid systems and interfaces stability of dispersions through polymer and surfactant adsorption*. CRC Press (2009).
30. Lisuzzo L, Cavallaro G, Parisi F, Milioto S, Lazzara G. Colloidal stability of halloysite clay nanotubes. Ceramics International **45**, 2858–2865 (2019).
31. Ruhsing Pan J, Huang C, Chen S, Chung Y-C. Evaluation of a modified chitosan biopolymer for coagulation of colloidal particles. Colloids and Surfaces A: Physicochemical and Engineering Aspects **147**, 359–364 (1999).
32. Cheng N-S. Effect of concentration on settling velocity of sediment particles. Journal of Hydraulic Engineering **123**, 728–731 (1997).
33. Wilson MJ. The origin and formation of clay minerals in soils: past, present and future perspectives. claymin **34**, 7–25 (1999).
34. Joussein E, Petit S, Churchman J, Theng B, Righi D, Delvaux B. Halloysite clay minerals – a review. claymin **40**, 383–426 (2005).
35. Rawtani D, Agrawal Y. Multifarious applications of halloysite nanotubes: a review. Rev Adv Mater Sci **30**, 282–295 (2012).
36. Keller WD, Matlack K. The pH of clay suspensions in the field and laboratory, and methods of measurement of their pH. Appl Clay Sci **5**, 123–133 (1990).
37. Theng BKG, Wells N. The flow characteristics of halloysite suspensions. claymin **30**, 99–106 (1995).
38. Hogg RI. Mutual Coagulation of Colloidal Dispersions. Trans Faraday Soc **162**, 1638–1651 (1966).
39. Van Oss CJ. *Interfacial forces in aqueous media*. CRC press (2006).
40. Palomino AM, Santamarina JC. Fabric map for kaolinite: Effects of pH and ionic concentration on behavior. Clay Clay Miner **53**, 211–223 (2005).
41. Sutherland BR, Barrett KJ, Gingras MK. Clay settling in fresh and salt water. Environmental Fluid Mechanics **15**, 147–160 (2015).
42. Chen Q, Cho H, Manthiram K, Yoshida M, Ye X, Alivisatos AP. Interaction potentials of anisotropic nanocrystals from the trajectory sampling of particle motion using in situ liquid phase transmission electron microscopy. ACS central science **1**, 33–39 (2015).

43. Katana B, Takacs D, Csapo E, Szabo T, Jamnik A, Szilagyi I. Ion Specific Effects on the Stability of Halloysite Nanotube Colloids-Inorganic Salts versus Ionic Liquids. J Phys Chem B **124**, 9757–9765 (2020).
44. Li X, Li H, Yang G. Promoting the Adsorption of Metal Ions on Kaolinite by Defect Sites: A Molecular Dynamics Study. Sci Rep **5**, 14377 (2015).
45. Jackson ML. *Soil chemical analysis: Advanced course*. UW-Madison Libraries Parallel Press (2005).

Declarations

Acknowledgements

The research described in this study was financially supported by National Research Foundation of Korea (NRF) grant funded by Korea government (MSIP; Ministry of Science, ICT & Future Planning) (NRF-2021M3H4A6A02050365) and a grant from the Water Management Research Program funded by the Ministry of Land, Infrastructure, and Transport (MOLIT) of the Korean government (21AWMP-B114119-06). We would like to thank Editage (www.editage.co.kr) for English language editing.

Author contributions

N.N., Y.M.K., K.S.D., G.C.C., I.C., and J.M.Y. designed the concepts and experiments. Y.M.K., conducted the sedimentation test and calculated the interparticle interaction energy. N.N. and K.S.D. performed in-situ LPSEM, LPTEM, and LPOM analysis. N.N. and Y.M.K. prepared the manuscript with K.S.D. under supervision of G.C.C., I.C., and J.M.Y.

Competing interests

The authors declare no competing interests.

Figures

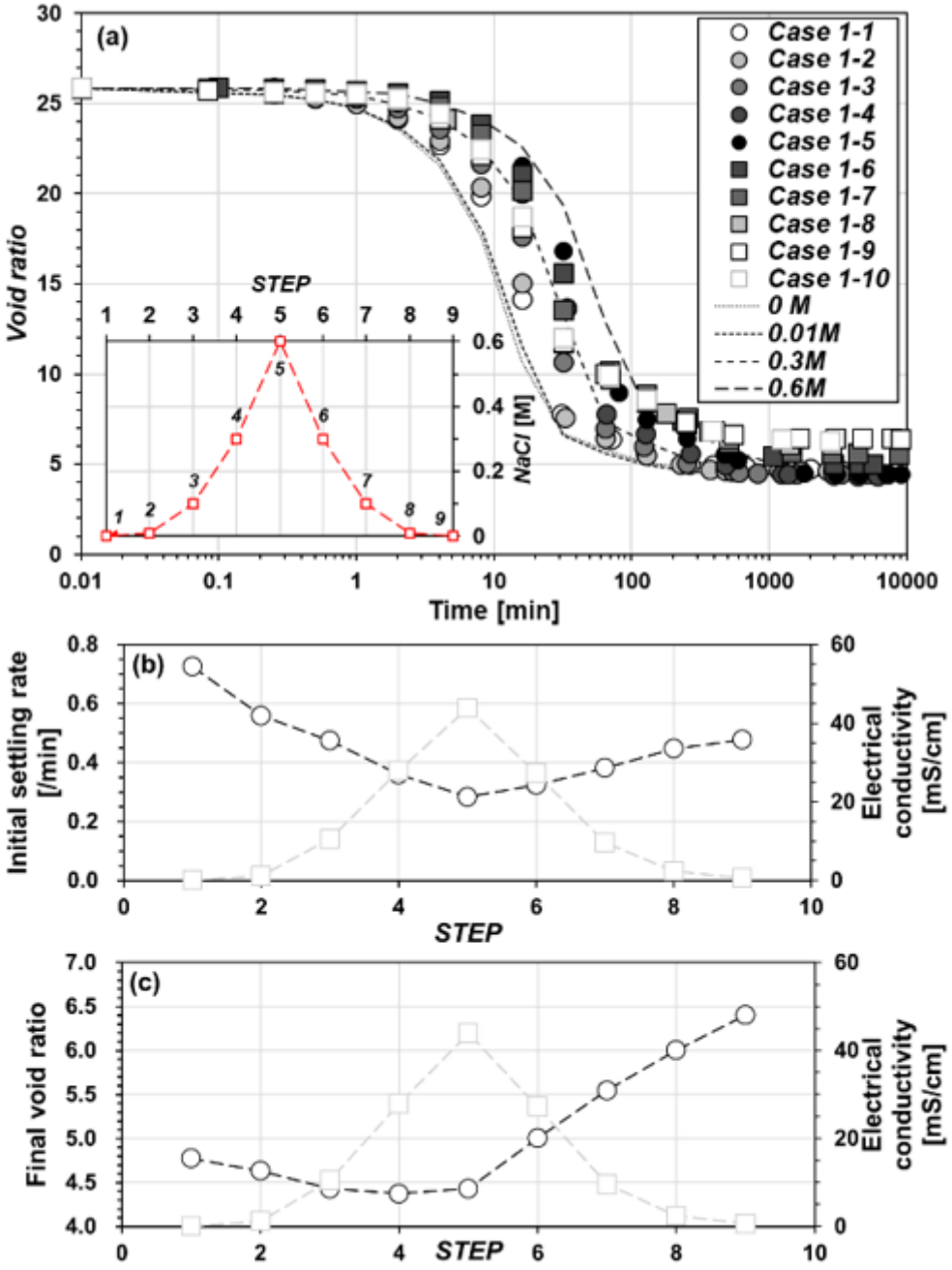

Figure 1

Settling behavior and electrostatic interaction of halloysite clay nanotubes. a the variation in void ratio as a function of time and salinity during the sedimentation of HNTs from salination (0 M to 0.6 M) to desalination (from 0.6 M to 0.01 M), **b** the initial settling rate, and **c** the final void ratio.

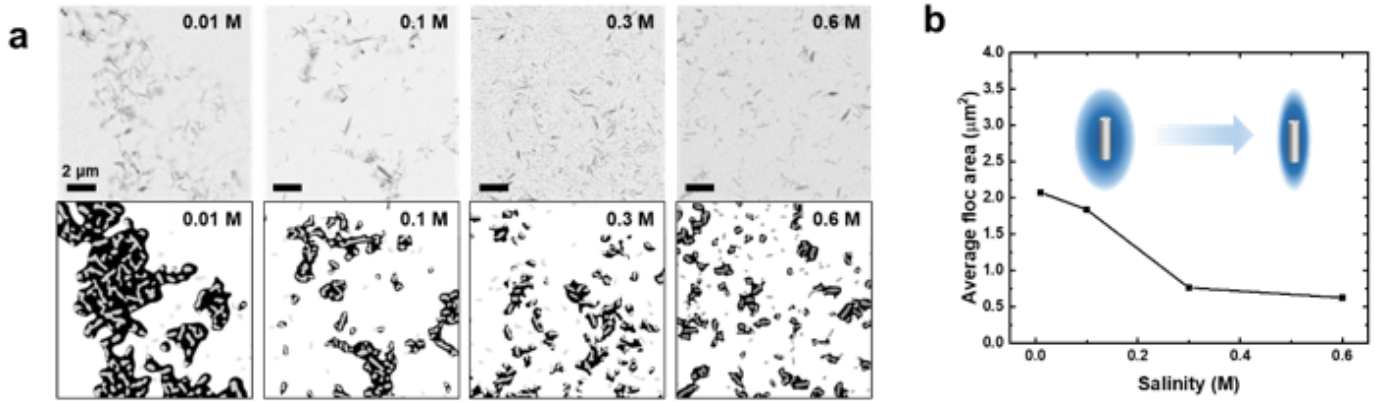

Figure 2

HNT associations at different initial salinity observed by using the *in-situ* LPSEM. a Microscopic structures of the flocculated HNTs. Upper panels are representative SEM images at individual salinity (0.01 M, 0.1 M, 0.3M, and 0.6M) and bottom panels are processed images corresponding to upper SEM images, respectively. **b** Average floc size extracted from processed SEM images at different salinity levels.

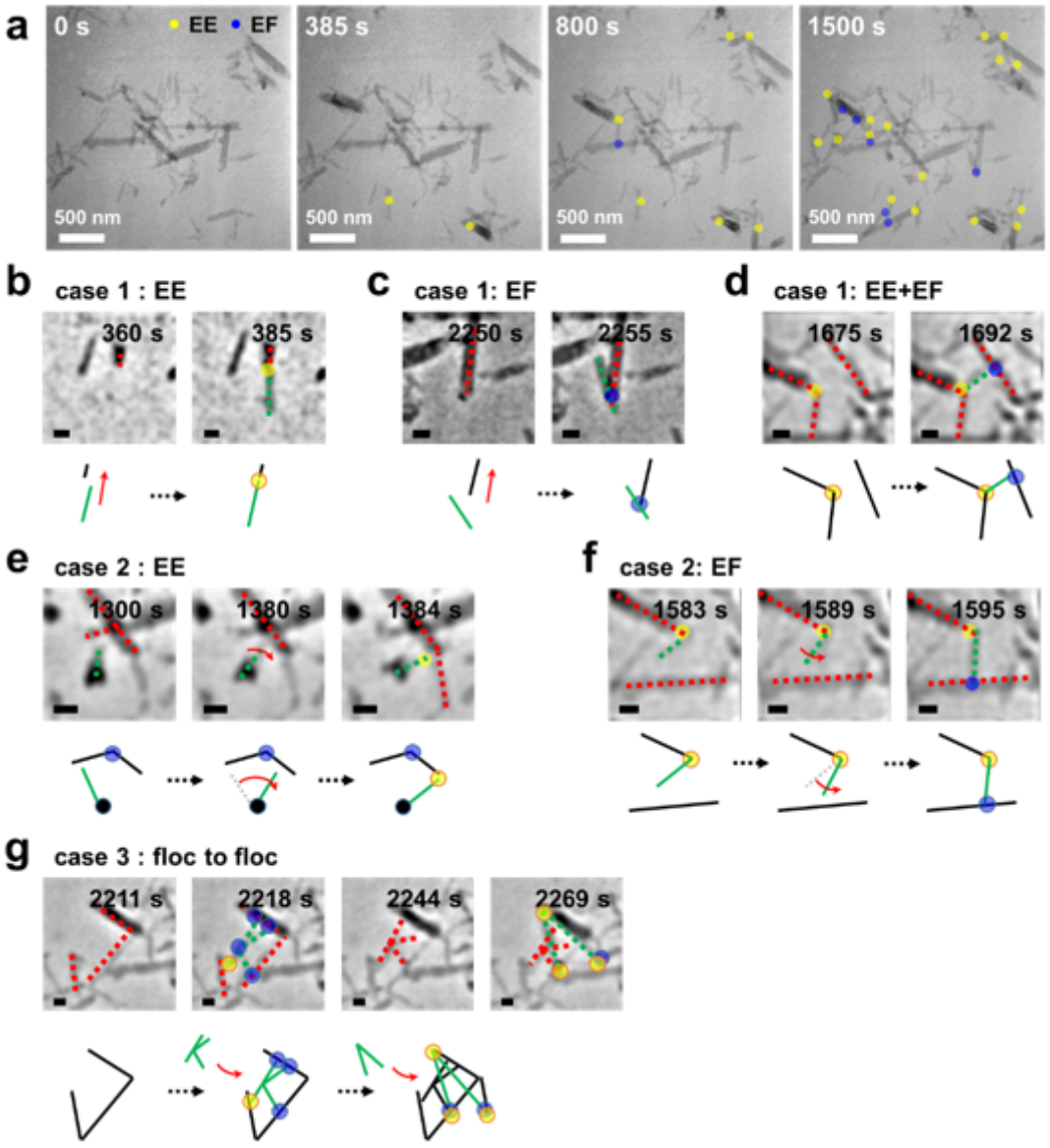

Figure 3

HNT interaction and possible flocculation pathway in pure water. a Initial flocculation process of the individual HNTs identified using *in-situ* LPTEM at t = 0 s, 385 s, 800 s, and 1500 s. **b-g** Sequential TEM images and the schematic diagrams as particular HNT assemblies for time-dependent HNT interaction in pure liquid. Case 1: In most cases, **b** EE, **c** EF, and **d** both formation processes by direct attachment of individual HNTs particles. Case 2: **e** EE and **f** EF formation process by attachment of moving particle. Case 3: **g** multiple floc to floc formation process by attachment of foreign aggregate formed in the flow channel. In the figure, yellow and blue dots indicate the newly formed EE and EF association points, respectively. Red dotted lines represent the pre-existing particle, and green dotted lines represent the attached particles on it. The scale bars in figure **b-g** are 100 nm.

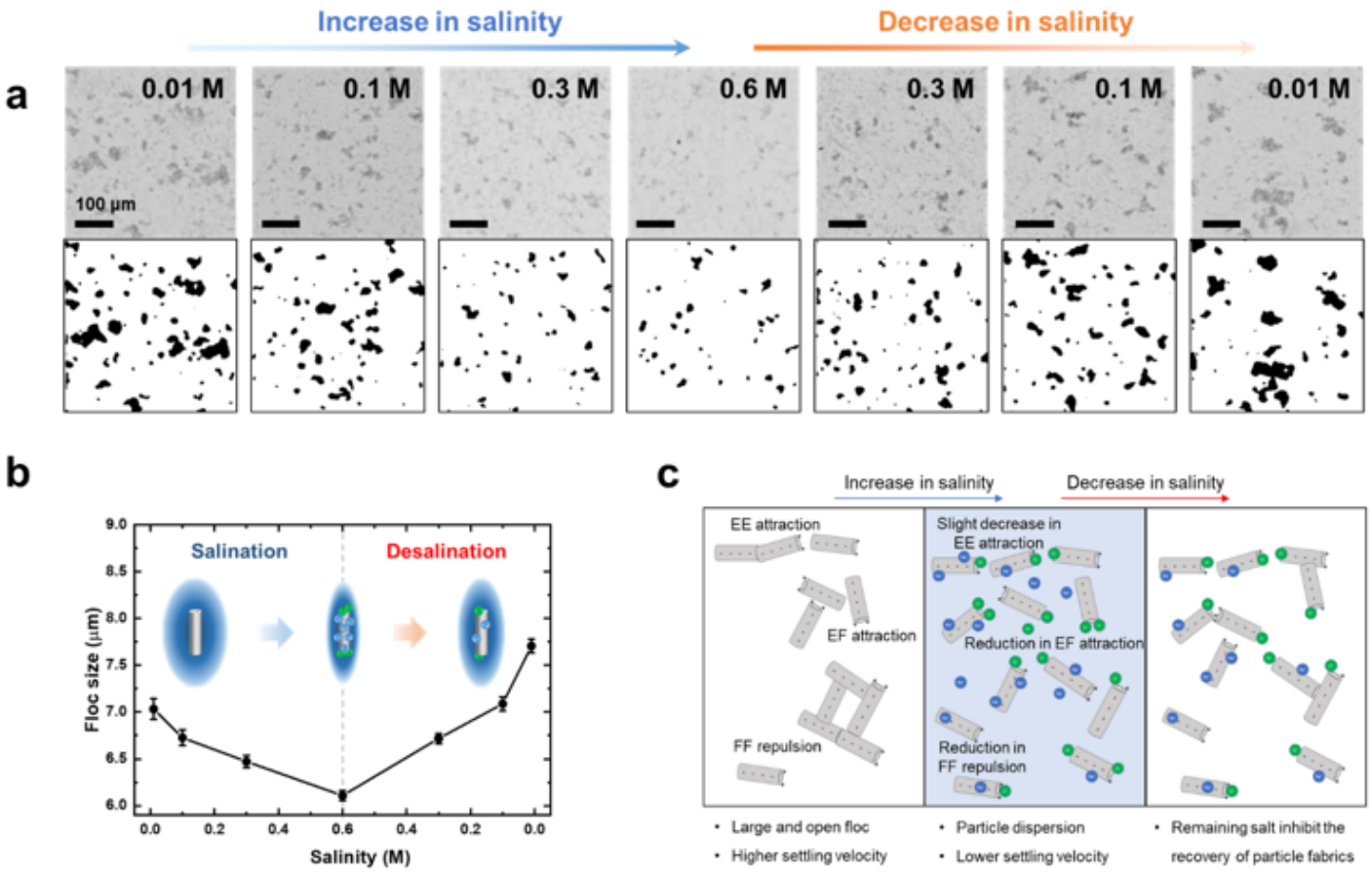

Figure 4

Aggregates formation via a series of salination and desalination. a Serial LPOM images of conglomerated fabrics during exchange condition from salination (0.01 M to 0.6 M) to desalination (0.6 M to 0.01M). Upper panels are representative OM images and bottom panels are processed images corresponding to upper OM images, respectively. **b** The calculated diameter of aggregates with changes in salinity extracted from processed OM images. **c** The summary of particle interaction via a series of salination and desalination. Blue and green spheres indicate the Na^+ and Cl^- ion, respectively.

Supplementary Files

This is a list of supplementary files associated with this preprint. Click to download.

- Supplementaryinformation.docx
- Video13ax60.mp4
- Video23bx60.mp4
- Video33cx30.mp4
- Video43dx30.mp4

- Video53ex12.mp4
- Video63fx301.mp4
- Video73gx30.mp4
- Video8s10ax12.mp4
- Video9s10bx28.mp4